Astron. Astrophys. 317, 125–139 (1997)

ASTRONOMY
AND
ASTROPHYSICS

Near-simultaneous X-ray and optical observations of the RS Canum Venaticorum binary SV Camelopardalis

A. Hempelmann[1], **A.P. Hatzes**[2], **M. Kürster**[3], **and L. Patkós**[4]

[1] Astrophysikalisches Institut Potsdam, An der Sternwarte 16, D-14482 Potsdam, Germany
[2] McDonald Observatory, The University of Texas at Austin, Austin, Texas 78712-1083, USA
[3] Max-Planck-Institut für extraterrestrische Physik, Giessenbachstr., D-85748 Garching, Germany
[4] Konkoly Observatory of the Hungarian Academy of Sciences, H-1525 Budapest XII, Box 67, Hungary

Received 8 June 1995 / Accepted 18 May 1996

Abstract. We report on a multi-wavelength campaign of optical and X-ray observations of the short-period eclipsing RS CVn binary star SV Cam. We present an X-ray light curve measured by ROSAT in Aug. 93, two V-band light curves obtained in Sep. and Nov. 93, and Doppler imagery based on high-resolution spectroscopy of photospheric absorption lines observed Sep.–Nov. 93. The total X-ray output of the SV Cam *binary* was found to be on a level typical for *single* main sequence stars. Thus SV Cam does not appear to be overactive, contrary to what is generally claimed for RS CVn systems. We model the X-ray light curve with two extended coronal emission regions. One region is located above a photospheric region of the primary star where spots have frequently been observed and where we find evidence for photospheric spots from our optical data. The second X-ray source in our model is located between the two components of the binary. Our Doppler image shows a distinct spot on the primary star centred at a stellar latitude of 60°. This spot is also found in an analysis of the optical light curve observed in September. A second spot in the Doppler image, which appears as an appendage to the main feature, seems to be spatially correlated with the second X-ray source. While our analysis yields no evidence for this feature in the September light curve it clearly determines the November light curve indicating rapid evolution of an active spotted region. Furthermore, we find evidence of strong (chromospheric) activity on the secondary star of SV Cam. During secondary eclipse the strength of the Hα absorption line of the single-lined binary increases by a much larger factor than can be accounted for by continuum light (or lack thereof) from the secondary indicating strong Hα emission from the secondary star. Also during primary eclipse absorption features from the secondary star become visible in all photospheric lines except Hα which argues strongly for the lack of Hα absorption and, hence, for the appearance of significant amounts of Hα emission in the secondary star.

Send offprint requests to: Alexander Hempelmann (e-mail: ahempelmann@aip.de)

Key words: stars: activity – stars: coronae – stars: imaging – stars: RS CVn variables – X-rays: stars

1. Introduction

The observation of magnetically induced activity on late-type stars is surely among the most important discoveries of modern astrophysics. Empirical studies which relate the characteristics of stellar activity (photospheric spots, chromospheric plages, and a hot X-ray emitting corona) with basic stellar parameters such as mass, age, and rotation are a natural way to test dynamo theories. A large number of observations have demonstrated the fundamental importance of stellar rotation for the generated activity level whereas the relation between turbulence and stellar activity has not yet been well determined observationally. Another parameter affecting the observed activity levels is stellar age. It is well established that younger stars are more active than older ones which is probably a result of their more rapid rotation rate (see Pallavicini 1989, and references therein). On the one hand this view is supported by the fact that old stars which are forced into rapid rotation through tidal interaction in *binary systems* – such as the RS CVn stars – also exhibit high levels of activity. On the other hand slowly rotating young stars of the solar type are simply not known.

The question whether binary stars represent their own class of magnetic activity has not yet been answered unambiguously. The often used statement in literature that RS CVn stars are "overactive" suggests another quality of dynamo action than that responsible for the activity levels of single stars. However, it seems obvious that another kind of dynamo could only be the result of tidal forces on the plasma motions in the stellar interior which are thought to be responsible for the appearance of stellar magnetism and activity.

With a separation of only three stellar radii between the two components (Hilditch et al. 1979) SV Cam is one of the closest

binary systems among the class of RS CVn stars. Hence, tidal interaction will be much stronger in this system than for most of the other RS CVn binaries. We can expect, therefore, a maximum difference between the observed activity of SV Cam and the activity level typical for the sum of two single stars having the same stellar parameters as the components of SV Cam. Thus, SV Cam is a very suitable candidate to answer the question whether RS CVn stars represent a separate class of stellar activity or not. We will address this issue by a comparison between the expected X-ray luminosities of two single main sequence (MS) stars with appropriate stellar parameters and the observed total X-ray output for SV Cam found in this paper. For this comparison we will use the relation between coronal X-ray emission and Rossby number given by Hempelmann et al. (1995).

The system parameters of SV Cam were determined by eclipse studies and by spectral line analysis (Hilditch et al. 1979; Patkós 1982; Budding & Zeilik 1987; Patkós & Hempelmann 1994). The two MS stars are of spectral types G2–3V and K4V. They have an orbital period of 0.6 days and a ratio of their radii of 0.64. The G-type primary whose rotation period can be determined photometrically is known to be in synchronous rotation, which certainly can be assumed also for the K-type secondary. This, together with the inclination angle of exactly 90° allows us to pursue another question: which is the location of the X-ray emitting regions within the stellar corona of SV Cam? And, are both components magnetically active?

As both stars have the same rotation periods, their levels of coronal activity can be expected to be similar. If this is the case, a minimum should be visible in the X-ray light curve during secondary eclipse when the secondary star is totally occulted by its primary companion. During primary eclipse, on the other hand, the primary star is exclusively occulted in its equatorial region providing a possibility to constrain the latitude of its active regions. As is known from Doppler imaging studies magnetically active regions in several RS CVn stars occur preferably at high latitudes or in the polar region – at least on the photospheric level. Examples are HR 1099 (=V711 Tau; Vogt 1988; Donati et al. 1992), UX Ari (Vogt & Hatzes 1991) and EI Eri (Strassmeier 1990). In this case a large fraction of the X-ray emitting regions on the primary star may remain unocculted during primary eclipse which then could not produce a deep minimum in the X-ray light curve.

This scenario precisely describes the results from studies of the totally eclipsing RS CVn binary AR Lac made with three different X-ray observatories. Observations made with the *Einstein* satellite were interpreted in terms of two distinct coronal emission components to be present, one of them compact and located close to the stellar surface(s) and the other more extended and comparable in size to the radius of the larger star to which it was found to be associated (Walter et al. 1983). Subsequent observations of AR Lac with EXOSAT were also explained by two plasma components, a compact one identified with relatively cool thermal plasma of $\approx 7 \times 10^6$ K and a very extended one, pervading the whole binary system in this model, and identified with hot plasma of $\approx 1.4 \times 10^7$ K (White et al. 1990). Finally, Ottmann et al. (1993) found the same two plasma components in a ROSAT PSPC observation of AR Lac but determined their respective extents to be similar to the *Einstein* result, with the cool ($\approx 3 \times 10^6$ K) component compact and the hot ($\approx 1.4 \times 10^7$ K) component associated with the larger star and comparable in size with its radius.

While eclipse studies can provide information on the spatial distribution of coronal emission regions, it is still an open question whether the photospheric spots observed on active late-type stars are connected with magnetic field structure in the form of loops as frequently observed on the Sun. First attempts at investigating this interrelation of photospheric and coronal active regions were made by Kürster & Dennerl (1993) for the active stars AB Dor, CF Tuc, and YY Men. These authors compared ROSAT PSPC light curves with contemporaneous photospheric Doppler images finding the observations to agree with the concept that X-ray emitting loops connect the major star spot complexes. However, there are many uncertainties in these models, and confidence in this picture will only be built, if it manages to explain more observations.

If the general picture borrowed from the Sun, i.e. from a relatively inactive star, is valid also for RS CVn-type and related stars, then the coronal emission regions should have a tendency to be located in the proximity of spot complexes which can be seen in Doppler images. Simultaneous or quasi-simultaneous observations in the X-ray and optical spectral regions are required to address this issue. We define a set of observations as "quasi-simultaneous" (or "contemporaneous"), if it is carried out within a time interval short enough that no substantial reconfiguration of the distribution of active regions must be expected, at least on the photospheric level on which the evolution of active regions apparently is slower. In this paper, we will present the results of quasi-simultaneous observations of SV Cam.

A description of our observational basis will be given in Sect. 2. These observations will be analysed in Sect. 3. Sect. 3.1 is about the coronal activity of SV Cam. A comparison with the X-ray luminosities of single stars, a temperature estimate, short-term variability like possible flare events and periodic modulations of the X-ray light curve are the contents of Subsects. 3.1.1–3.1.4. In Sect. 3.2 our optical photometric observations are modelled on the basis of one circular spot. Sect. 3.3 is an interpretation of spectral line profile variations in terms of star spots. It includes Doppler imagery from four spectral lines in Sect. 3.3.1, the influence of line blending on those results in Sect. 3.3.2, and a comparison of such found stellar surface distributions of spots with both the estimated positions of coronal sources (Sect. 3.3.3) and the spot found from optical light curve modelling (Sect. 3.3.4). While these results concern the primary star of the SV Cam binary, the line profile variations of H_α will be interpreted in terms of activity of the secondary star in Sect. 3.4. A summary and some conclusion will be given in Sect. 4.

2. Observations

We observed SV Cam in the soft X-ray region of the spectrum with the ROSAT PSPC (bandpass 0.1–2.4 keV). The instru-

Table 1. Phase-binned X-ray data

Phase	counts/sec	Error
0.047	0.325	0.013
0.073	0.417	0.023
0.156	0.348	0.013
0.182	0.429	0.018
0.288	0.375	0.021
0.364	0.385	0.012
0.390	0.398	0.014
0.407	0.385	0.013
0.490	0.394	0.012
0.517	0.370	0.014
0.549	0.468	0.022
0.612	0.374	0.012
0.642	0.341	0.016
0.706	0.410	0.011
0.733	0.424	0.014
0.750	0.396	0.016
0.815	0.450	0.016
0.851	0.424	0.015
0.934	0.400	0.022
0.958	0.394	0.018

Table 2. Spectroscopic Observations

JD 244	Phase	Exp [min]	S/N
9288.895	0.456	20	130
9288.933	0.520	20	130
9288.993	0.622	20	140
9289.008	0.647	20	160
9321.809	0.954	20	110
9321.839	0.004	20	110
9321.908	0.121	20	240
9321.983	0.247	20	200
9321.998	0.272	20	130
9322.842	0.696	20	230
9322.934	0.851	20	210
9322.974	0.918	20	175
9357.031	0.343	20	170

Table 3. Spectral Lines for Doppler Imaging

λ (Å)	Species	χ (e.V.)	EW (mÅ)
6102.8	Ca I	4.08	252
6122.0	Ca I	1.89	211
6400.0	Fe I	3.60	435
6439.1	Ca I	2.52	223

ment and the satellite are described by Pfeffermann et al. (1986) and Trümper et al. (1991), respectively. The observations were carried out in August 1993 between JD 2,449,225.332 and JD 2,449,229.056. The total exposure time was 34.5 ksec distributed over eleven exposures of length half an hour and seven exposures lasting only a few minutes. This observational run was over 3.5 consecutive SV Cam binary orbits. (Consecutive observations minimise any distortion of the orbital or rotational light curve by intrinsic variability which has their origin in the physical appearance and disappearance of X-ray sources in the stellar corona.) It follows a gap of two days in the observations. The time-series was then finished by a single 15 min exposure.

The data reduction was done with the help of the EXSAS software package (Zimmermann et al. 1994) and included corrections for dead time and telescope vignetting. In a first step for the production of a light curve the photon counts were binned into time-intervals of maximum length 200 sec. Then these data were folded with the following ephemeris given by Patkós (1982):

$$JD_{\rm o} = 2,433,777.42453 + 0.5930718E \quad (1)$$

where $JD_{\rm o}$ is the time of the primary star eclipse. The resulting X-ray light curve count-rate vs. orbital (= rotation) phase shows a nearly regular sequence of phase intervals covered by observations (of different epochs) and gaps between them. Typical lengths of those nine phase intervals of observations are 0.02–0.07. The gaps are of similar length. In the next step we binned the observations in phase intervals of ≈ 0.02 to reduce scatter in the light curve. These values are given in Table 1 and the light curve is shown in Fig. 1.

Our contemporaneous optical observations were planned subject to the ROSAT schedule on which we had no influence. Unfortunately, because of bad weather conditions in Central Europe and a too large zenith distance for SV Cam as observed in the southern U.S.A. in August 1993, it was not possible to observe the star in an exactly simultaneous manner. One month later (JD 2,449,254–57) it was observed photometrically in the V-band at the Piszkéstető Mountain Station of the Konkoly Observatory Budapest with the 50 cm reflector. The V-band light curve is shown in Fig. 2 (filled circles). Its out-of-eclipse asymmetry reveals an expressed maculation effect caused by star spots. A second V-band light curve was observed in November (JD 2,449,310–11). It is also shown in Fig. 2 (open circles). As is evident from the figure the maculation effect in this second light curve is strongly reduced. These observations are part of a photometric long-term monitoring program on SV Cam which was begun in 1973 by LP. The results of the first decade were published by Patkós (1982).

Spectral observations were made on 28/29 Oct. 1993, 30 Nov./01 Dec. 1993, and one spectrum was obtained on 03 Jan. 1994. Due to SV Cam's position in the sky and pointing restrictions of the telescope it was only possible to follow SV Cam for a few hours at the end of the night in late October. This, along with an inclement weather, made it necessary to acquire data over a much longer time base than was desired.

The Sandiford Cassegrain Echelle spectrograph at the McDonald Observatory 2.1 m telescope was used. This instrument is a prism cross-dispersed Echelle that is used with a 1200×400 Reticon CCD, and it provides large wavelength coverage at high (up to $R \approx 60{,}000$) resolving power (McCarthy et al. 1993). The instrumental setup for the SV Cam observations yielded a wavelength coverage from 5850 to 7250 Å with a resolution of 0.17 Å (3 pixel slit) at 6400 Å, corresponding to $R = 38,000$. In order to minimise phase smearing exposure times were limited to 20 min.

Table 2 lists the journal of observations for the spectral data. This includes the Julian day of the observations, the rotation phase (ϕ) according to the ephemeris of Equ. 1, exposure time in minutes, and the signal-to-noise (S/N) per CCD pixel.

3. Results

3.1. Coronal activity

3.1.1. Total X-ray luminosity

Before discussing the X-ray light curve we want to compare the total X-ray output of the RS CVn binary SV Cam with that of single stars. For single main-sequence stars we know the relationship between coronal activity on the one side and rotation and stellar structure on the other side. The latter two parameters can be combined in the Rossby number Ro:

$$Ro = P_{\rm rot}/\tau_{\rm c} \tag{2}$$

where $P_{\rm rot}$ is the stellar rotation period and $\tau_{\rm c}$ the convective turnover time at the bottom of the convection zone. For stars with Rossby numbers smaller than one, Hempelmann et al. (1995) find linear relationship between the X-ray stellar surface flux, $F_{\rm X}$, and Ro:

$$\log F_{\rm X} = 5.80 - 0.97 \log Ro \tag{3}$$

where $F_{\rm X}$ is expressed in erg s^{-1} cm^{-2}. There, the convective turnover times ($\tau_{\rm c}$) were taken from the paper by Stępień (1989):

$$\begin{aligned} \tau_{\rm c} &= 20.5 \qquad \text{if} \qquad B-V \geq 0.8 \\ \tau_{\rm c} &= -21.3 + 53(B-V) \qquad \text{if} \qquad B-V < 0.8 \end{aligned} \tag{4}$$

The 1σ scatter of the individual data points around the regression curve of Equ. 3 was found to be $\log F_{\rm X} = 0.35$ (Hempelmann et al. 1995) which implies an uncertainty of a factor of two in any prediction of a X-ray count-rate from that relation. This uncertainty is a likely result of X-ray variability and coronal activity cycles as Hempelmann et al. (1996) have suggested.

The spectral types of the two stellar components (see Sect. 1) imply $B-V = 0.65$ and 1.05 for the primary and the secondary star, respectively (cf., Lang 1974). Hence, from Equs. 3 and 4 and a rotation period of 0.59 d resulting from the assumption of tidal coupling of the stellar rotation with the orbital motion, we expect $\log F_{\rm X} = 7.1$ for the primary star and $\log F_{\rm X} = 7.3$ for the secondary star. With $v \sin i = 117$ km s^{-1} (see Sect. 3.3), $i = 90°$, and $r_2/r_1 = 0.64$ (Patkós & Hempelmann 1994) we find the radii of the two stars to be $r_1 = 1.3$ R$_\odot$ and $r_2 = 0.8$ R$_\odot$. We thus obtain $\log L_{\rm X} = 30.1$ and $\log L_{\rm X} = 29.9$ (in erg s^{-1}) for the primary star and for its companion, respectively. The total output is then expected to be $\log L_{\rm X} = 30.3$. With a distance of 74 pc (Strassmeier et al. 1993) and a flux-to-count-rate conversion factor of 1.7×10^{11} ct cm^2 erg^{-1}, typical for stellar coronal sources, a count-rate of 0.50 ct s^{-1} is expected in the PSPC bandpass (0.1–2.4 keV).

From our ROSAT pointed observation we find a mean count-rate of 0.395 ± 0.004 ct s^{-1} for SV Cam. Dempsey et al. (1993), using the ROSAT all-sky survey data, determined a count-rate of 0.41 ± 0.04 ct s^{-1} for the same star. Taking into account the uncertainty in the prediction we find it to be in excellent agreement with the observation. We conclude that the observed level of coronal activity of the binary SV Cam is not enhanced in comparison to single stars. This is in agreement with the general conclusion for RS CVn stars made by Dempsey et al. (1993) who did not find any correlation between the Roche lobe filling fraction, which is a measure of the tidal forces between the stellar components, and the level of coronal activity. Both results are in contradiction to the finding by Montesinos & Jordan (1988) that, for a given rotational period, binaries show a higher $F_{\rm X}$ than single stars.

3.1.2. Coronal temperature and electron density

We also analysed the X-ray spectrum of SV Cam. On the basis of a Raymond-Smith thermal plasma the spectrum can be explained with a two temperature model, $T_1 = 3 \times 10^6$ K and $T_2 = 1.5 \times 10^7$ K. These are the same values as found for the well-studied RS CVn star AR Lac (White et al. 1990, Ottmann et al. 1993). This is a bit surprising because AR Lac shows an almost one order of magnitude higher X-ray luminosity than SV Cam (Dempsey et al. 1993).

To determine the electron density (n) from the emission measure $EM = n^2V$ we need to know the volume (V) of the coronal sources. Unfortunately, this parameter is undetermined (cf., Sect. 3.1.3.2), thus the electron density cannot be estimated.

3.1.3. Non-periodic variability

X-ray studies of the Sun like that carried out by *YOHKOH* (cf., Tsuneta & Lemen 1993 and references therein) have demonstrated that strong variability ranging from minutes to days is typical for the solar coronal activity on the shorter time-scales. This short-term variability has its origin in dynamical processes inside the magnetic plasma above an active region. If this is also typical for much more active stars such as SV Cam then the intrinsic variability can dominate over the variability caused by eclipses through a stellar companion or self-eclipses caused by the stellar rotation. A possible test is to compare the count-rates which were observed at one and the same phase of the binary orbit but at different orbital cycles. SV Cam has been observed in rapid succession by ROSAT (in most cases ≈ 30 min exposures in ≈ 90 min succession) over more than three cycles of its binary motion and after further three cycles without observations a last 15 min exposure was done. Hence, phase overlapping of observations made at different times is expected. Indeed, we find ten overlaps. In seven of these cases identical count-rates have been observed which let us conclude that any kind of short-term variability on the X-ray light curve caused by eclipses and stellar rotation will not be dominant.

However, in three cases enhanced activity has been found: neither other observations at the same phase nor observations at neighbouring phases can reproduce their high level of activity. Unfortunately, all these three data points are of somewhat ex-

traordinary nature: two points at the phases 0.07 and 0.18 result from extremely short exposures lasting only a few minutes (the usual exposure time was half an hour) which make it impossible to find out the real nature of their enhanced count-rates. The third point at phase 0.55 results from the last (isolated) exposure. We cannot decide whether the coronal activity was enhanced over that whole binary cycle or was the result of variability on a short time-scale. However, the latter idea is supported from the observation of an increasing count-rate during the 15 minutes. The count-rate at the end of that exposure was a factor 1.5 higher than at the beginning.

These three data points were therefore regarded as isolated events and were consequently rejected from the analysis described in the next section.

3.1.4. Rotational modulation and eclipses

3.1.4.1 Choice of a model

In order to explore the information content of the X-ray light curve with respect to the spatial structure of SV Cam's corona we first consider the model that both stellar components have homogeneously radiating coronae of negligible height so that eclipses of the corona(e) should occur in the same phase intervals as eclipses of the photosphere(s). In this case the following two features should be apparent in the light curve: First, a total eclipse of the secondary star should be observed centred on phase 0.5 and with a reduced count-rate of 0.25 ct s^{-1}. This is clearly not seen in the light curve of Fig. 1. Second, the annular eclipse of the primary star would lead to a slightly shallower minimum ($\approx$ 0.30 ct s^{-1}) centred on phase 0. There actually is a solitary low data point at phase 0.047 indicating a related eclipse event. Unfortunately though, the sparse sampling and the rather large level of fluctuation in the light curve make it impossible to infer the shape and exact phase of the suggested minimum. However, the general impression one obtains from Fig. 1 by considering also the light curve modulations near the quadrature phases is such that minima in the X-ray curve occur at phases later than the mid-eclipse of the stellar photospheres. This implies an inhomogeneous distribution of emission regions in SV Cam's corona.

At first we have to determine the minimum number of isolated emission regions which can fit qualitatively the complexity of the light curve. Can the light curve be explained by rotational modulation and eclipses of a single localised X-ray emitting region? Assuming that the emitting plasma is optically thin and provided that the structure of the emission region is not too complex, its rotation induced self-occultation would produce a fairly symmetric light curve with a shape between a step function and a sinusoidal curve – depending on the extent of the region. In addition, an eclipse of the source by the companion star could be superimposed. It is immediately evident that the observed light curve shape is more complex so that at least two distinct emission regions are required to explain it. We will be satisfied with that model if the light curve is fitted on a level of confidence of 95% or better.

Table 4. Solutions of X-ray model parameters

Par.	DC=0.0 ct/s	DC=0.1 ct/s	DC=0.2 ct/s
h	0.80R$_*$	0.45R$_*$	0.3R$_*$
$l1$	15°	30°	24°
$b1$	14°	19°	20°
$\alpha 1$	65°	65°	60°
$cr1$	0.204 ct/s	0.172 ct/s	0.120 ct/s
$l2$	239°	254°	250°
$b2$	5°	20°	15°
$\alpha 2$	57°	52°	43°
$cr2$	0.231 ct/s	0.180 ct/s	0.114 ct/s
χ^2	13.6	14.0	14.4

h: (lower) height of a source above the surface of the primary star;
l: stellar longitude calculated as $l = \phi \cdot 360$ and ϕ the orbital phase
b: stellar latitude calculated from the equatorial plane of the primary star
α: angular radius of the X-ray emitting region parallel to the primary star surface
cr: X-ray count-rate of the single source

For the quantitative analysis on the basis of that two features model we have used the code written by MK (see Ottmann et al. 1993 for a first application). This code allows us to devise corona models with a specified number of emission features which consist of truncated coni with spherical boundaries concentric to the surface of one of the stars. We used coni with a circular cross-section, but other shapes can be chosen. If a feature is viewed as a sequence of spherical layers of increasing height, each layer has the same emissivity. In this modelling approach there are the following free parameters per feature: stellar longitude and latitude, angular radius, lower and upper height above the surface of the respective star (the lower height need not be the stellar surface), and the X-ray flux arising from the feature (in ct sec^{-1}). A final model parameter which we denote as "*DC* component" is the constant fraction of the light curve and results from any additional emission region that remains unaffected by the binary star geometry. Examples are a very extended emission "halo," a distant feature located outside of the orbital plane of this $i = 90°$ binary, or an uneclipsed and symmetrical polar cap on the primary star.

The need to constrain the number of free parameters lead us to fix the vertical extent (upper height minus lower height) of both features to 0.2 primary star radii. In addition we placed both features at the same height above the primary star.

3.1.4.2 Parameter optimising

In the modelling procedure we have explored wide ranges of the parameter space to find corona models with an acceptable fit quality in terms of the χ^2 given by

$$\chi^2 = \sum_{i=1}^{N} \frac{(cr_i^{\rm calc} - cr_i^{\rm obs})^2}{\sigma_i^2} \qquad (5)$$

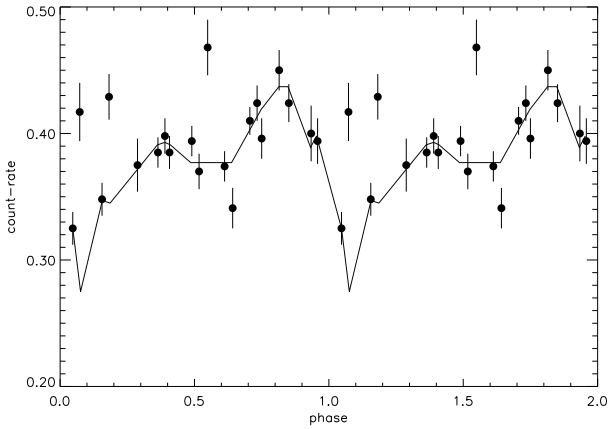

Fig. 1. X-ray light curve observed with the ROSAT PSPC in August 1993, together with a best fit model comprising two coronal sources whose parameters are given in Table 4, column 2 (DC = 0.0 ct s^{-1}). These sources are schematically represented in Fig. 10.

where $cr_i^{\rm obs}$ and $cr_i^{\rm calc}$ denote, respectively, the individual observed and calculated (from the model) count-rates, σ_i denotes the measurement error and N the number of data points. This task of finding acceptable models is an optimisation problem with local minima usually corresponding to very different coronal configurations. Thus uniqueness of the model is not warranted a priori. We chose as our criterion to accept a given model that the chance probability of exceeding its value of χ^2 must be $> 5\%$ or, conversely, that the confidence for its rejection must be $< 95\%$. In a fit of 10 parameters to 17 data points (7 degrees of freedom) our confidence criterion corresponds to a reduced χ^2 of ≤ 2.01 or $\chi^2 \leq 14.1$. We managed to find only one minimum of χ satisfying our criterion. Table 4 shows the resulting fit parameter near this minimum for three different values of the DC component. Column 2 of this table, pertaining to $DC = 0$, shows our best fit model at the absolute minimum of χ^2. Our model with DC = 0.1 (3rd column) is also acceptable. The DC = 0.2 model (4th column) just fails to satisfy our criterion. As it reaches a $\chi^2 \approx \chi^2_{\rm min} + 1$ it provides the 1σ error of the DC component.

It is clear from Table 4 that all the parameters are more or less strongly correlated with each other leading to a relatively large interval of a parameter uncertainty which is much greater than in the uncorrelated case. The strongest correlation exists between DC and h. Therefore, and because the relation between them is unambiguous – in contrast to the relation between l_1 and h, for instance – we have decided to list in Table 4 the solutions of the other parameters in dependence on DC.

The range of possible values for DC faces a hard upper boundary due to the fact that this parameter must not exceed the observed count-rate. There is no corresponding hard lower boundary (other than $DC \geq 0$). The value of DC is determined in an interplay of all parameters to account for the geometrical conditions while at the same time producing the observed X-ray flux. For example, with increasing DC the two parameters cr_1 and cr_2 must decrease to keep the observed count-rate of ≈ 0.4 ct s^{-1}. Another strong correlation, namely between DC and h, is of geometrical nature. The higher a source is located above the photosphere of the primary star the larger is the fraction of the X-ray emitting volume which is visible at each phase. This fraction produces a constant contribution to the observed count-rate – it thus acts like a DC component. These mutual compensation effects can operate merely within certain limits. For example, if cr_1 and/or cr_2 fall below a certain level then the absolute amplitude of eclipse or self-occultation events pertaining to the corresponding feature will be reduced below the observed value. As a consequence, the whole model light curve becomes flatter leading to a degraded fit. This is the case when DC exceeds (or when h or cr_1 and cr_2 fall below) the values of column 4 in Table 4. The best model with DC = 0.3 is 6σ above the minimum χ^2 model. Thus we find a possible range of the height of the coronal sources between $\approx$0.3R$_*$ and 0.8R$_*$. Note, however, that additional uncertainties result from the simplifying assumptions of an identical height of the two sources and a fixed radial thickness of 0.2R$_*$.

A formal attempt was made to find a reasonable range of solutions for the volume. However, reducing the radial thickness of a source from 0.2 R$_*$ to 0.02 R$_*$ changed the value of χ^2 only marginally from 13.6 to 13.7. Hence, the uncertainty of the volume is at least three orders of magnitude and more. This prevents not only any meaningful determination of the X-ray emitting volume but also the estimate of the electron density (cf., Sect. 3.1.2).

3.2. The optical light curve

In Fig. 2 we show the optical V-band light curve folded with the ephemeris of Equ. 1. Data points obtained in September and November 1993 are depicted by solid circles and open circles, respectively. As a solid line the eclipse model derived by Patkós & Hempelmann (1994) is also shown. The eclipse curve was calculated using the computer code by Budding (1973) and Budding & Najim (1980).

As is obvious from Fig. 2, there is a significant deviation between the pure eclipse model corresponding to two spotless stars and the observed photometry. Fig. 3 shows the difference curve for the September data. It looks typical for a rotationally modulated light curve of a single dark spot. Consequently, we fit these observations assuming a single spot of circular shape to be present on the surface of the primary star. (The secondary star cannot produce the observed curve of Fig. 3, because its contribution to the total light in V is too small to explain its amplitude.) The spot modelling procedure is described in detail in the papers by Hempelmann & Schöneich (1987) and Patkós & Hempelmann (1994). The main difference to the code of Budding & Najim (1980) is that we consider the contrast q of the circular spot as a free parameter as well (q represents the ratio of the mean flux densities inside and outside of the circular spot). This is done because it is not known whether the active region is a single spot or a group of spots interspersed with bright photospheric areas. In the latter case, q represents a combination of contrast and spot filling factor inside the circular

Table 5. Model solutions for the optical light curve observed in September 1993. In all cases the stellar longitude is determined to be $l = 78^\circ \pm 2^\circ$.

	single spot			double spot	
b	α	q	ΔT	q	ΔT
(0°)	45°	0.91	115 K	–	–
(10)	44	0.90	130	0.95	65
(20)	42	0.89	145	0.94	70
(30)	40	0.87	170	0.94	85
40	37	0.81	255	0.90	120
50	30	0.68	450	0.84	210
55	26	0.50	750	0.75	340
60	22	0.22	1435	0.61	560
70	15	–	–	0.00	5750

b: stellar latitude;
α: angular spot radius;
q: flux density ratio spot-to-spotless surface;
ΔT: temperature difference photosphere minus spot derived from q by use of Planck's law;
if $b > 70^\circ$: no solution because of negative q's;
if $b < 40^\circ$: no solution because no spot occultation is visible in the light curve during primary eclipse;
Columns 3 and 4 correspond to single spots centred on one hemisphere whereas columns 5 and 6 pertain to double-spot solutions mirror-symmetrical with respect to the equator.

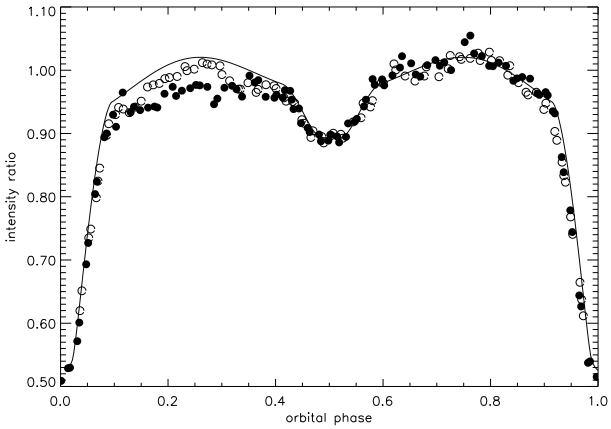

Fig. 2. V Light curve of SV Cam observed in September (solid circles) and November (open circles) 1993. The solid line represents the expected curve for a pure eclipse model.

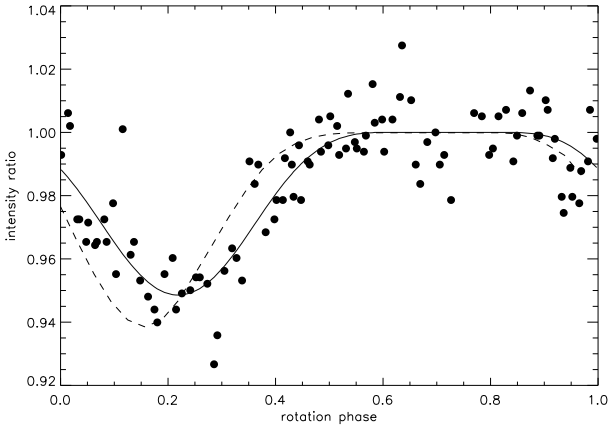

Fig. 3. Difference curve between the eclipse fit and the observations from September 1993. The solid line is the model curve based on the parameters given in Table 5, row 7. The dashed line represents the model curve derived from the Doppler image shown in the top panel of Fig. 6. If the Doppler image is modified in such a way that the appendage (at longitude 40°) to the dominant spot is removed (see Sect. 3.3), the predicted curve becomes almost indistinguishable from the shown solid line.

region. Also, we do not have information on the spot temperature which requires measurements of the colours V–R or V–I (cf., Vogt 1981).

The stellar longitude of the spot is well-constrained by the data. We find $l = 78^\circ \pm 2^\circ$; i.e. the spot centre passes the line of sight at phase 0.22. According to our analysis in Sect. 3.1.3.2 one of the two coronal X-ray sources is located about 50° from this spot. In Sect. 3.3.3 we will discuss the connection of this X-ray source and the photospheric spot with a common active region.

As a consequence of taking q as a free parameter the stellar latitude and the spot radius cannot be determined unambiguously. All three parameters are strongly correlated so that a range of solutions results for each of them. In Table 5 the solutions for spot radius α and contrast q are given depending on the possible stellar latitudes b. Stellar latitudes larger than 70° are forbidden, because negative values of q would be required for a solution which is physically impossible. The possible spot radii range from 45° for spots at the equator down to 15° for spots at $b = 70^\circ$. However, as no spot occultation effect is visible during primary eclipse in the light curve of Fig. 3 we can restrict our solutions to the intervals $30^\circ \lesssim b < 70^\circ$, corresponding to $40^\circ > \alpha > 15^\circ$. In Table 5 the temperature difference between the spot and the spotless photosphere (whose temperature is 5750 K) is also given (4th column).

In the case of an inclination angle between the rotation axis and the line of sight of 90° (assuming the rotation axis to be perpendicular to the orbit) there is an additional ambiguity between solutions at b and $-b$. Furthermore, both positions can be occupied with spots leading to the same light curve as for the single spot (see also the discussion in Sect. 3.3.1). Therefore, we show in Table 5 the single spot model (Cols. 3 and 4) together with the double spot solutions that are symmetrical with respect to the equator (Cols. 5 and 6).

The small amplitude of the spot-induced photometric wave observed in November makes it difficult to determine the same number of free parameters as can be inferred from the September curve. However, the November data show a minimum in the photometric wave at phase 0.10 corresponding to a spot position of $37^\circ \pm 7^\circ$ in stellar longitude. This is significantly smaller than the value derived from the September data and implies some kind of spatial reconfiguration within the active region. Furthermore, the amplitude of the photometric wave in the November light curve has less than half the value of the

September curve showing the star brighter at wave minimum while its brightness is unchanged at wave maximum. This indicates that the spot contrast and/or the spot coverage must have decreased considerably.

3.3. Photospheric structures

3.3.1. Doppler imaging

A Doppler image of the photospheric spot distribution on SV Cam was derived using the maximum entropy method (MEM). The details of the reconstruction technique, which is constrained to find only cool spots, can be found in Vogt et al. (1987). The signal-to-noise of the SV Cam spectral data is much lower than is typically used for Doppler imaging studies. SV Cam is a single-lined binary for which mutual blending of the absorption line systems of the two components is not a problem (see, however, Sect. 3.4). But unfortunately, the rotational velocity of the spectroscopically visible primary star is so large that blending of neighbouring lines within its spectrum is of greater concern than for the more slowly rotating RS CVn-type stars. This blending can alter the shape of the spectral lines and thus affect the derived spot distribution.

In order to minimise the effects of blending, four spectral lines were used in the Doppler reconstructions: Ca I 6103 Å, Ca I 6122 Å, Fe I 6400 Å, and Ca I 6439 Å (for more information, see Table 3, which provides the excitation potential χ and equivalent width EW of the lines). These features in the SV Cam spectra appeared to be relatively blend-free. However, a comparison to the solar spectrum showed that the Ca I 6103 Å line has Fe I lines 0.5 Å on either side of it. Both of these Fe lines are almost as strong as the Ca line. The Fe I 6400 Å line is blended with a weaker Fe I line at 6400.3 Å. The only unblended lines seem to be the Ca I 6439 Å and Ca I 6122 Å lines. Doppler reconstructions were performed using the blended lines as well so as to gauge what effects blending has on the final Doppler images and to see if the gross features of the spot distribution were reproduced in spite of blending problems. The effects of blending will be discussed in Sect. 3.3.2

Of the 13 collected spectra (Table 2) only those 11 were used that were not observed during primary eclipse. For the Doppler imaging reconstructions a stellar inclination of 90° was chosen. The $v \sin i$ of the star was measured from the four spectral lines used in the Doppler reconstructions. A high signal-to-noise profile for each line was produced by co-adding all the observed phases (except for those taken during primary eclipse). A fit to these profiles using synthetic spectral lines yielded a mean $v \sin i = 117 \pm 3$ km s^{-1}. This value together with $i = 90°$ and $P_{\rm rot}$ = 0.6 day yields a stellar radius of the primary star of 1.3R$_\odot$ implying that it is somewhat more evolved than the Sun.

Local spectral line profiles used in the Doppler reconstruction were generated using ATLAS5 routines and Kurucz's model atmospheres (Kurucz 1979). A macroturbulent velocity of 4 km s^{-1} was also included in the modelling.

Fig. 4 shows the Doppler images of the spot distribution using the four spectral lines. These images are shown as grey-scale representations in 'pseudo-Mercator' (latitude vs. longitude) projection. The darkest regions have temperatures approximately 1000 K below the photosphere and the lightest grey shade that is visible represents a temperature 250 K below the photosphere. Fig. 5 shows the observed spectral line profiles as vertical bars and the predicted line fits as a solid line for each of the spectral lines used in the reconstructions. The size of each vertical bar represents a $\pm 1\sigma$ error in the flux measurement.

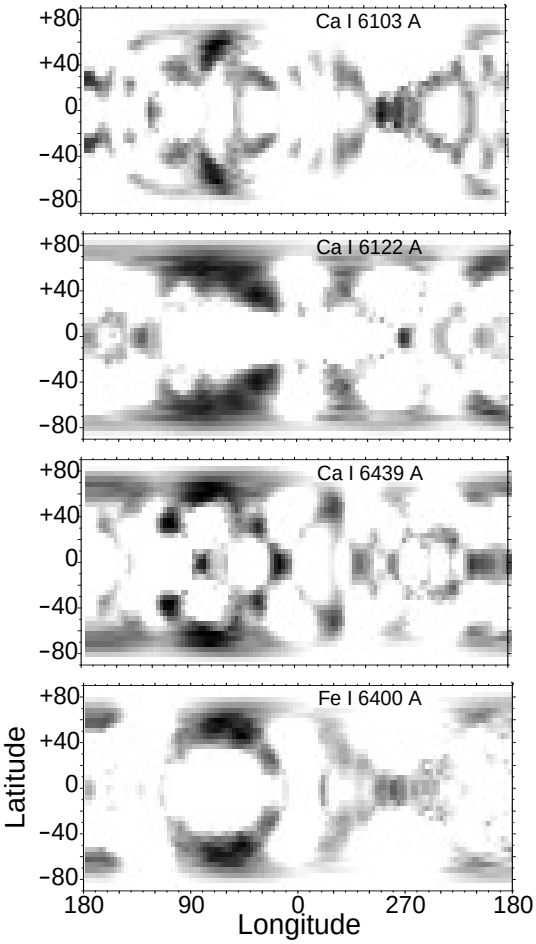

Fig. 4. The Doppler images derived using (top to bottom) Ca I 6103 Å, Ca I 6122 Å, Ca I 6439 Å, and Fe I 6400 Å. They are shown in 'pseudo-Mercator' projection (latitude vs. longitude).

Note the mirroring about the stellar equator in each of the Doppler images, an artifact due to the high inclination of the star. For a star with inclination of 90° there is complete ambiguity as to the sign of the latitude for a spot feature (the absolute magnitude of the latitude is well determined). Thus the true location of a spot feature may be in either hemisphere, or both. Although it seems improbable that a spot will have a mirror 'companion' in the opposite hemisphere, such a distribution can still fit the data and thus cannot be excluded. To simplify the following discussion, spots will be considered to lie only in the "northern hemisphere" (i.e. at positive latitude) but the reader should keep in mind that the sign of the latitude is not known.

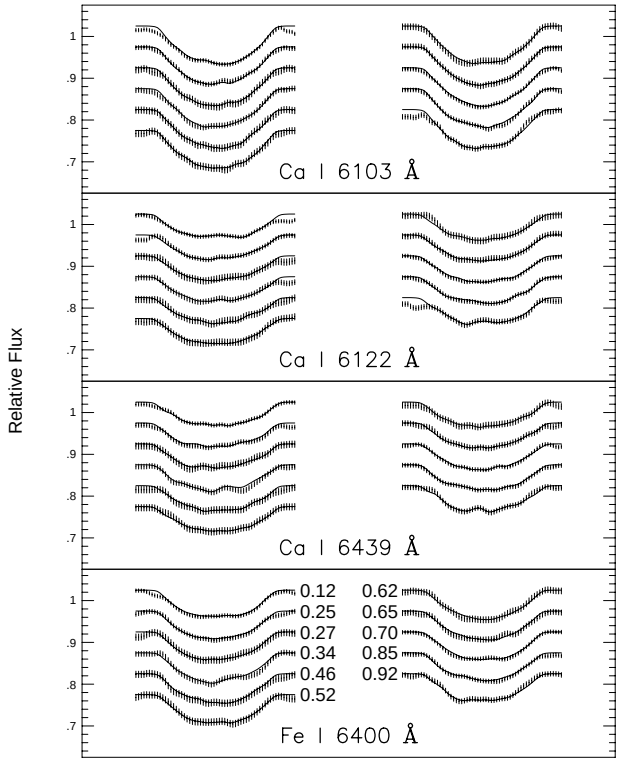

Fig. 5. The observed spectral line profiles (vertical bars) and fits from the Doppler images (solid line) for (top to bottom) Ca I 6103 Å, Ca I 6122 Å, Ca I 6439 Å, and Fe I 6400 Å. The length of each vertical bar represents a $\pm 1\ \sigma$ error in the flux measurements. The numbers by the profiles in the lowest panel indicate the rotation phase for the profiles (same ordering in all panels).

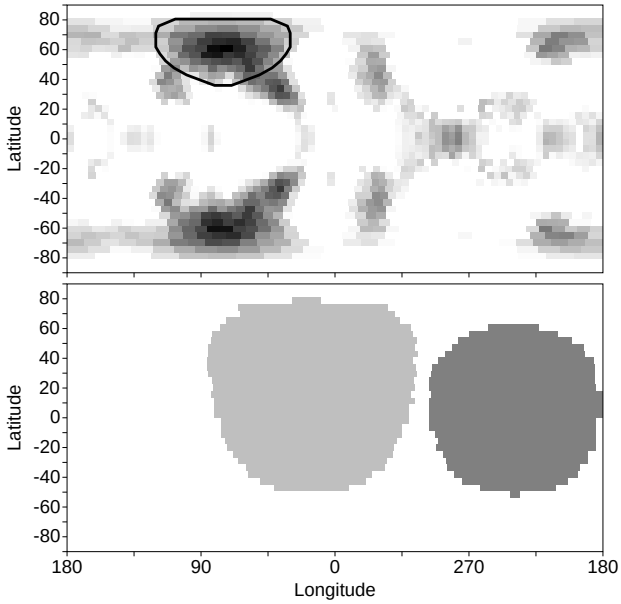

Fig. 6. (Top) The Doppler image that results after averaging the four individual maps in Fig. 4, again in grey scaled 'pseudo-Mercator' projection. The solid line indicates the location and size of the spot derived from the 1993 September photometry. (Bottom) The X-ray map derived from the parameters of Table 4, Col. 2. Here, the darker region represents the more luminous one.

The top panel of Fig. 6 shows the Doppler image that results after averaging the individual maps. The heavy solid line indicates the size and location of the spot derived from the September 1993 photometry. Among the several possible models of Table 5 the single-spot model with $b = 60°$ was chosen which implies a temperature difference from the photospheric value that is most consistent with the spot temperature inferred from the Doppler image (see discussion in Sect. 4).

The spot distribution on SV Cam is dominated by a strong, almost circular spot near longitude 75° and latitude +60° which has an appendage near longitude 40° that extends down to latitude +30°. This feature appears to be quite robust being present in all four Doppler images at roughly the same low brightness level (i.e. a very cool feature). Other features in the images are only marginally cooler than the photosphere. Even though many of these features appear in all four maps, they are somewhat suspect due to their relatively high temperatures, the low signal-to-noise in the data, and the subtlety of the distortion features in the observed spectral line profiles.

3.3.2. Effects of line blends

The fact that all four Doppler images seem to recover the same gross features of the spot distribution, namely the strong circular spot near latitude 75°, would seem to indicate that line blending does not introduce large errors in the Doppler image. There are some differences between the individual Doppler images, but it is not clear that these are due to blends. For instance, the image from the unblended Ca I 6122 Å line is most similar to the image from the slightly blended Fe I 6400 Å line. The Ca I 6103 Å (strongly blended) has similarities to both the Ca I 6439 Å image (unblended) and the Fe I 6400 Å image (slightly blended). It seems that gross errors in the assumption of the local line profile are unimportant and that the rotational velocity of SV Cam is so high that it dominates the shape of the observed profile thus minimizing the effects of nearby blends. In fact, the rotation broadening substantially exceeds the separation of the close blends in all cases. One only needs a very approximate shape for the local line profile and this seems to be adequately provided by a profile for a single line (without blends) generated by model atmospheres. Furthermore, to zeroeth order, the primary effect of blends is a slight increase in the spectral line width and this can be compensated by an appropriate choice of $v \sin i$. (The rotational velocities measured from the Ca I 6103 Å and Fe I 6400 Å line are 117 km s^{-1} and 115 km s^{-1}, respectively. The fact that these values are near the mean for all four lines may suggest that the blending for these lines may not be as severe as that inferred from the solar spectrum.) Most likely, the differences seen between the various Doppler images result from noise in the data.

3.3.3. Comparison to the coronal sources

The lower panel of Fig. 6 shows a map of the coronal sources with the parameters derived from the analysis of the X-ray light curve in Sect. 3.1.3.2 (Table 4, Col. 2). Note that, contrary to the Doppler image, this map is a negative representation in which the *darker* colour corresponds to the *stronger* X-ray flux. From Fig. 6 it seems that the centre of one X-ray emission region is located above the appendage to the polar spot. The second X-ray feature is centred above the low-level equatorial photospheric spot at longitude 270°. Even though this equatorial spot is a marginal feature in the Doppler images, the fact that the inferred location of one of the X-ray sources is so near suggests the existence of an active region on this part of the stellar surface so that this spot may indeed be a real photospheric feature. In the average Doppler image this equatorial spot is only about 300 K cooler than the photospheric temperature. In several of the individual Doppler images (Fig. 4), however, this feature is much more prominent. In the Ca I 6103 Å image it is nearly as cool as the high-latitude spot. It is also reasonably strong in the Fe I 6400 Å image with a temperature 500 K below the photospheric value. In the Ca I 6122 Å image it is even cooler (about 700 K below the photosphere), but has a much smaller size. In fact the only image in which this equatorial spot does not appear is the Ca I 6139 Å map. This image does show several low-level spots surrounding the location of the equatorial spot. Interestingly, the longitudinal location on the star coincides with one that has historically shown considerable spot activity (cf., Zeilik et al. 1988). We caution, however, that this spot feature appears strongest in the maps derived with the Ca I 6103 Å and Fe I 6400 Å lines, the two lines with the highest degree of line blending. The appearance of weak features could thus be an artifact of the blending.

3.3.4. Comparison to the light curve

In Fig. 3 SV Cam's V-band light curve (with the eclipse effects removed) of September 1993 is compared with the light curve predicted from the average Doppler image. Observations are shown as circles whereas the curve derived from the photometric modelling is shown as a solid line. The predicted light curve from the average Doppler image is indicated by the dashed line. In producing the predicted light curve from the Doppler image the following assumptions were made.

1. All spot features were considered to be located in the northern hemisphere.
2. The Doppler image (which has a smooth transition between spotted and photospheric regions) was converted into a two-temperature distribution. Image pixels with a temperature less than some threshold to be determined (see 3rd item) were assigned a temperature value of 1200 K below the photosphere (a typical value found for several RS CVn stars). Image pixels with a temperature greater than this were assumed to be unspotted regions and therefore assigned the photospheric temperature of 5750 K.
3. The proper threshold value was determined such that the amplitude of the photometric wave as seen in the September light curve was fitted. This yielded a suitable threshold value of 5350 K (or 400 K below the photospheric temperature).

The applied threshold preserved only the most robust features of the Doppler image, namely the high-latitude circular spot and its appendage. Note that our assumption that all features are located in only one hemisphere does not affect the shape of the predicted light curve as a spot feature located in either hemisphere produces identical light curves for a star with 90° inclination. If a spot had a mirror companion in the opposite hemisphere, then both spots would have to be much warmer in order to fit a given photometric amplitude.

Our choice to fit the amplitude of the September light curve rather than that of the November light curve is somewhat ad hoc. It was led by the fact that both the Doppler image and the September photometry reveal the large spot at longitude 75° as their dominant feature. Besides the amplitude (which was fitted by using a suitable threshold) also the shape of the observed light curve is reproduced quite well by the predicted one, although there appears to be a phase shift of about $\Delta\phi \approx 0.07$ between the two. After eliminating the appendage to the polar spot one obtains a predicted light curve almost coincident with the solid line derived from the photometric modelling of the September data. This does not prove, however, that the appendage (which may actually be located in the opposite hemisphere and may not be physically associated with the polar spot) is not a real feature. The September 1993 light curve was observed more than a month before the spectral data, and real changes in the spot distribution have likely occurred in the interim. The light curve observed in November 1993 (which is much closer to the spectroscopy) has its minimum at phase 0.10 which corresponds to a spot position coincident with the appendage in the Doppler image. From September to November the light curve also appears to have undergone a decrease in amplitude as well (for a more detailed discussion, see Sect. 4).

3.4. Activity of the secondary star

The large wavelength coverage of the Sandiford Echelle made it possible to acquire data simultaneously on Hα. These spectral profiles were examined to see if any rotational modulation which may be an indication of surface plage could be detected. Fig. 7 shows the variations of this spectral feature in SV Cam. These profiles include the two spectra observed near the beginning and middle of the eclipse of the primary star (phases 0.954 and 0.004) which were not used in the Doppler reconstructions. Note the strong distortion (emission-like bump) visible at phase 0.004 in the red wing of the profile. As this emission-like bump is seen in all photospheric lines we consider a transient event such as a flare as an unlikely cause. We interpret this feature as resulting from the obscuration of part of the primary star by its darker secondary companion. In effect the shape of the Hα profile at this phase represents a Doppler "snapshot" of the eclipse (or transit). The secondary star with an estimated spectral type of K4 (Barrado et al. 1994) is considerably cooler than the primary

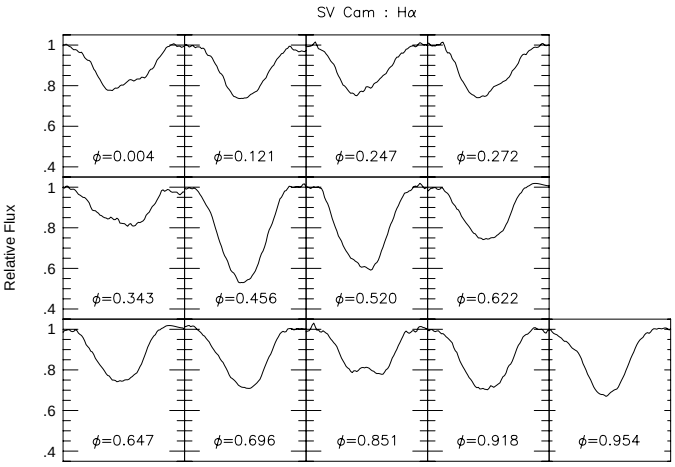

Fig. 7. The observed spectral line profiles for Hα.

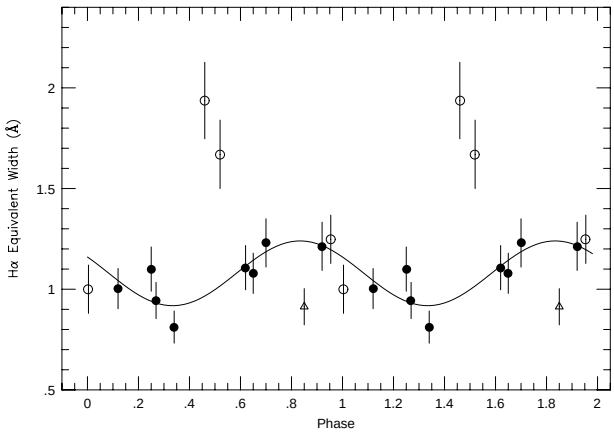

Fig. 8. The equivalent width variations for Hα as a function of rotation phase. Open circles represent data taken near primary or secondary eclipse. A possible transient event is depicted by an open triangle. The solid line represents a least squares sine fit to the data points represented by the solid circles.

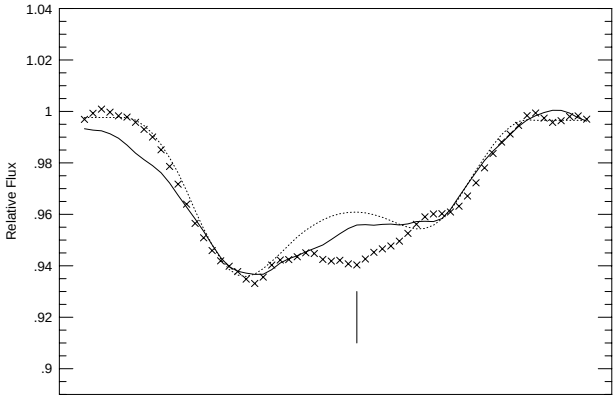

Fig. 9. The shape of the photospheric lines at primary eclipse (ϕ = 0.004). Crosses represent the mean shape of the 4 spectral lines used in the Doppler imaging reconstructions. The solid line is the observed Hα profile. The dashed line represents the predicted line profile shape of Hα assuming a secondary that is completely black. To facilitate comparisons the profiles have been re-binned and re-scaled so that all lines have roughly the same depth and width. The vertical bar indicates the location of a feature suspected to be due to absorption lines in the spectrum of the secondary star.

and when it transits it appears as a dark spot against the primary's surface. It thus masks part of the absorption line and produces a pseudo-emission distortion in the spectral line profile in the same manner as does a cool surface spot.

Fig. 8 shows the equivalent width variations of Hα. Open circles indicate data that were taken near primary or secondary eclipse. The triangle indicates a datum that is suspected to be a transient event (see discussion below). There is a strong increase in the absorption line strength at phases 0.456 and 0.520. Since at these phases the secondary star is eclipsed, we investigate the possible ways in which the observed increase in line strength can be caused by this eclipse event. First, we can rule out the assumption that the Hα line strength as it appears near secondary eclipse is comparable in both stars, as this would not lead to a change of the observed equivalent width during the eclipse events. Second, if the Hα absorption line of the secondary is filled in with emission up to the continuum level so that near 6563 Å the spectrum of the secondary is "flat" and the observed Hα absorption is caused solely by the primary star, then the measured equivalent width must increase during the total eclipse since the continuum-like light of the secondary is removed. However, the secondary's contribution to the total continuum flux amounts to only about 13% (inferred from the spectral types and radii of both stars) whereas during secondary eclipse the observed line strength of Hα increases by a factor of about 1.8. If this increase were due solely to removal of the continuum-like light of the secondary from the core of the absorption lines in the primary, then Fig. 8 would imply that the continuum level around 6563 Å for the secondary star is at least a factor of 1.6 higher than is expected for that star's spectral type. This strongly argues for a third possibility, namely that the light from the secondary at 6563 Å is in expressed emission, at least on a region of the secondary star located at phase 0.5. An emission scenario is in accordance with the smaller Rossby number of the secondary star (with respect to the primary) which can be inferred from the assumption of co-rotation with the orbital period. Hence, the secondary star is expected to be the star with the stronger chromospheric activity (cf., Noyes et al. 1984).

It seems that the light from the secondary can have a strong influence on the Hα line strength and this complicates interpretations of the Hα variations. Furthermore, there is some evidence for transient variations. Note in Fig. 7 the emission bump in the centre of the spectral line profile at phase 0.851 leading to a comparably small equivalent width of the line (data point represented as a triangle in Fig. 8). This bump is absent in the spectrum of phase 0.918 which was taken only one hour later. It is most likely due to a flare or some other transient event since a long-lived surface feature (e.g. plage) would still be visible in the line profile after a corresponding stellar rotation of only 24°.

When one eliminates the eclipse phases as well as the phase that is suspected to be a transient event (0.85) one does see some evidence of rotational modulation in the Hα equivalent width with a maximum occurring around phase 0.8. The best fit sine-wave is shown as a solid line in Fig. 8. The reduced χ^2 for the sine fit is decreased to 1.07 (at 5 degrees of freedom) from a value of 1.9 (at 7 degrees of freedom) that is provided by a straight line. Translated into confidence for rejection of either model we obtain 63% for the sine fit vs. 91% for the straight line fit.

Interestingly, the minimum of the modulation occurs around phase 0.3. If this decrease in strength is due entirely to emission filling in the core of Hα provided by surface features such as plage, then these features may be spatially associated with the strong photospheric spot found near phase 0.2. However, because of the suspected activity of the secondary it is difficult to judge if such variations are indeed due to surface features on the primary. If the secondary is the source of this variation then it implies enhanced activity of a region on the stellar surface which is located near the X-ray source lying between the two stellar components (see Fig. 10). An Hα emission region located near phase 0.3 (i.e. longitude 108°) on the secondary star would undergo occultation during secondary eclipse so that it may also be responsible for the strong increase in absorption line equivalent width near phase 0.5.

The line shape observed during primary eclipse also provides further evidence that Hα may be filled with emission in the companion star. The solid line in Fig. 9 represents the shape of the Hα profile at primary eclipse (ϕ = 0.004). The crosses show the mean shapes at this phase of the photospheric lines that were used in Doppler imaging. (To facilitate comparison the observed profiles have been re-scaled and re-binned so that they all have roughly the same depth and width). Also shown is a theoretical absorption profile for Hα (as a dashed line) which we calculated for the proper eclipse geometry assuming a secondary star that

1. either is completely dark and contributes no flux to the observed profile (in this case the theoretical profile for Hα is the dashed line in Fig. 9),
2. or has a completely filled in Hα line, i.e. a "flat" spectrum near 6563 Å.

Apart from an unimportant difference in line depth both assumptions lead to the same profile shape. Furthermore, under the same assumptions this profile shape constitutes also an excellent approximation to the predicted shape of the photospheric lines of other elements, since line broadening is completely dominated by rotation.

Note that the shape of the observed Hα profile is similar to that of the predicted profile – a pseudo-emission bump near line core. The mean shape of the photospheric CaI and FeI lines is markedly different. One can still see evidence for a pseudo-emission bump, but there is a superimposed absorption dip near line centre (marked by the vertical line). We interpret this feature as arising from absorption features in the spectrum of the secondary star. Normally, this star contributes only about 13% of the observed continuum flux. This level is too low for absorption features from the secondary to be easily detected in our somewhat noisy spectra. A careful search in the spectral data at out-of-eclipse phases revealed no features that could be clearly attributed to the secondary. During primary eclipse, however, the contribution of the secondary rises to about 26% of the integrated light facilitating the discovery of absorption features from the secondary star. Even in our spectrum taken at the onset of primary eclipse (phase 0.954) shallow secondary lines seem to be present in the blue wing of all metal lines.

As we have argued above that the increase of the Hα equivalent width during secondary eclipse can only be explained if one assumes that the secondary star has strong Hα emission arising from the occulted hemisphere. Our view of a chromospherically active secondary is further supported by the fact that no absorption dip similar to the one seen in the averaged metal lines is seen in the Hα profile at phase 0.004 (primary eclipse). However, the similarity of the observed and theoretical profiles of Fig. 9 indicates that at this phase the secondary star spectrum is close to "flat" (filled in absorption line) and does not exhibit expressed emission exceeding the continuum level. So there seems to be an inhomogeneous distribution of Hα emission regions (plage) present on the surface of the secondary which may also account for the rotational modulation of the Hα equivalent width induced from Fig. 8. In any case, we have strong evidence that the secondary star is chromospherically very active.

4. Summary and conclusions

With a separation of merely 3 primary star radii between the stellar components SV Cam is one of the closest binaries among the short-period class of RS CVn systems. It is therefore an ideal object to study the effects of strong tidal forces on magnetic activity.

As is shown in Sect. 3.1.1 the X-ray count-rate of SV Cam observed with the ROSAT PSPC lies slightly below the expected value derived from a relationship between $F_{\rm X}$ and the Rossby number Ro found by Hempelmann et al. (1995) for *single* MS stars. In that paper it was shown that the linear relationship found for stars with $Ro < 1$ agrees quite well with the prediction from dynamo theory. We conclude that the observed level of coronal activity of the binary SV Cam is not enhanced in comparison to single stars and we further conclude that the dynamo action in the stellar interior is not influenced by tidal forces. This is in agreement with the general conclusion for RS CVn stars made by Dempsey et al. (1993) who did not find any correlation between the Roche lobe filling fraction, which is a measure of the tidal forces between the stellar components, and the level of coronal activity. Both results are in contradiction to the finding by Montesinos & Jordan (1988) that, for a given rotational period, binaries show a higher $F_{\rm X}$ than single stars. However, the class of RS CVn stars is strongly inhomogeneous in their stellar parameters. Most stars of this class do not belong to the main-sequence. However, the relationships between activity and Rossby numbers for *single* subgiants and giants are unknown.

Hence, any kind of a comparison like done in this paper is at present not possible for the class as a whole.

The ROSAT X-ray light curve can be explained by a model of two localised coronal emission regions rather than by global emission coming from a homogeneously radiating stellar corona or from a common envelope of the two stars in the binary system. In our most probable model both sources of emission are located $0.80 R_*$ above the surface of the primary star which places one of the sources in a region central between the two stars (see Fig. 10). Therefore, it remains open whether this source has its origin in magnetism of the primary or of the secondary star, or whether it results from a possible interaction of the two stellar magnetospheres. Concerning the uniqueness of our corona model it must be noted that our mapping problem is highly ill-posed. Within our modelling assumptions we have exhausted the parameter space and found the best model which turned out to be unique for this special class of models. However, we cannot exclude the possibility of a corona more complicated in structure which could then also be confined more to the stellar surface(s). Nevertheless, such more complicated models must certainly have similarities with the one presented here which can be used as an indication that the X-ray activity is concentrated more towards the region between the binary components and less towards the far sides of the stars (see Fig. 10).

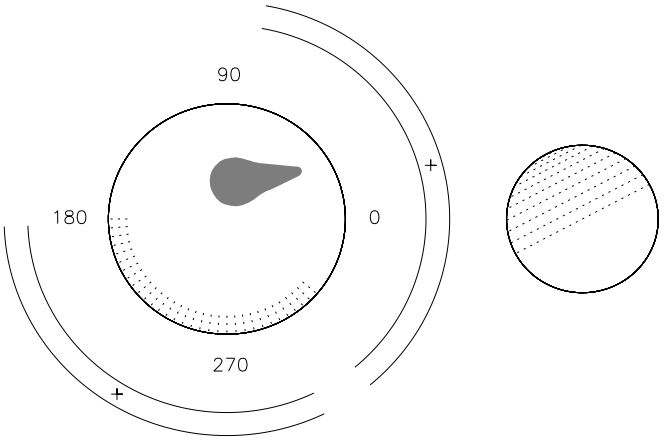

Fig. 10. *Schematic* pole-on view of SV Cam to illustrate the relations and positions of the binary components with respect to the magnetically active surface regions and the coronal X-ray sources. The centres of the two coronal features are marked with crosses. Black spot: feature found both from Doppler imaging and analysis of the V-band light curve; dotted region on the primary star: feature found only in the Doppler image. If the secondary star is the source of variability of the H_α emission then its dotted hemisphere is the more active one.

We find two photospherically active spot regions on the primary star. As our Doppler image demonstrates the first (and most expressed) active region is of complex nature. Its main structure is a large spot of almost circular shape. This spot was also found in our analysis of the September 1993 light curve, although there the spot latitude is not well constrained and ranging from between $\approx 40°$ to $70°$. If the temperature of the spots on SV Cam is typical for RS CVn stars (about 1200 K cooler than the photosphere; Eaton 1992), we can restrict the photometric solution to high latitudes which matches up well with the spot location inferred from the Doppler image. Cellino et al. (1985) derived for SV Cam a spot temperature of 1500 K which implies a stellar latitude very close to $60°$ (see Table 5). In Fig. 6 the agreement between the corresponding feature in the Doppler image and the photospheric spot solution for this latitude is demonstrated. There can be no doubt that this stellar feature is of real nature.

The light curve observed in September 1993 is completely explained with this spot alone. However, the Doppler image, based on spectra observed in late October (phases $0.445-0.647$) and late November (phases $0.696-0.272$; one spectrum at phase 0.343 was even observed in early January 1994) shows an additional feature in this active region: an appendage to the circular spot. Its reality is clearly established by the fact that it is found in the individual images pertaining to the four different absorption lines used. The whole active region is reminiscent of a bipolar Sun spot group consisting of an F spot and a P spot. However, one has to keep in mind that there is latitude ambiguity with respect to the equator, so that the circular spot may be in one hemisphere while the appendage is in the opposite hemisphere. This appendage is centred at longitude $40°$ or phase ≈ 0.1 and thus almost exclusively inferred from the spectra observed in late November. As demonstrated in Fig. 3 the presence of this appendage produces a noticeable change in the light curve, and this should have been detected if exactly simultaneous photometric measurements had been available. Our second photometric data set was obtained in mid-November, 12 nights before the relevant phase interval was observed spectroscopically. However, to complicate matters, on the one hand it reveals a minimum of the photometric wave at the phase of maximum visibility of the appendage, thereby lending credit to the view that it is a newly emerged star spot, on the other hand it does not yield any evidence for an expressed spot at longitude $78°$ which was clearly present earlier (in the September light curve) and also later (in the spectral line profiles of late November).

These different pieces of evidence can only be reconciled, if a rather complex scenario of disappearing and (re-)emerging or of migrating star spot is adopted. In this view the circular spot at longitude $78°$ dominates the photospheric spot distribution in mid-September; by mid-November this spot must have largely disappeared while a newly emerged second spot (the appendage at longitude $78°$) now prevails – alternatively, the first spot may have migrated to the new position while at the same time decreasing in either size or contrast; within another 12 days the previously dominant spot must have re-emerged (or a new spot must have emerged at the first position) being again the larger of the two spots (or spot groups).

Rapid evolution of the spot coverage and spot distribution on SV Cam seem to be part of this star's regular behaviour and were in fact previously observed (Patkós 1982; see also Tables 1 and 2 in the paper by Zeilik et al. 1988).

A second active region seen around longitude $270°$ in the Doppler image (top panel of Fig. 6) is of more speculative nature. It is less-expressed with respect to contrast and not visible to the same degree in all of the images produced from the

individual lines (Fig. 4). This suggests that it may be an artifact rather than a real stellar spot. However, there are strong arguments in favour of the reality of this feature. The first is its proximity to one of the two coronal X-ray sources located above its position and implying the existence of a magnetically active region. The second argument is based on the fact that this position of the stellar surface has often been observed to be a source of spot activity in the past. SV Cam is one of the RS CVn stars most extensively monitored by photometrists. Zeilik et al. (1988) analysed a fraction of this large data set consisting of 24 light curves observed between 1928 and 1984. They found spots to appear mainly in two regions centred around longitudes 90° and 270°. Sixty percent of the identified spots appeared in the latter region. One should note, however, that Zeilik et al. (1988) have restricted their analysis to symmetric light curves which can be explained by a single spot. Hence, quite naturally, they cannot find spots placed simultaneously at both positions. From a re-analysis of his own photometric data material, Patkós (unpublished) finds, however, that spots can frequently be found to occur at both positions at the same time. It seems that both regions are continuously active. Therefore we find it very likely that the second feature suggested from Doppler imaging and supported by the proximity of a coronal emission region really existed in late 1993.

The fact that spots can be found exclusively on the primary star does not imply inactivity or absence of spots on the secondary star. Because of the small contribution of the secondary to the total light of the binary evidence for spots on the secondary can neither be found in broad-band light curves nor in photospheric absorption lines. An exception is primary eclipse when the photospheric metal lines show additional absorption features narrower than the lines of the primary star which are believed to come from the secondary companion. However, no such absorption feature is seen in the Hα profile, which should be clearly present if the secondary were an inactive K4 star with Hα in absorption. It is thus implied that at primary eclipse the secondary spectrum (at the wavelength of Hα) closely resembles a flat continuum, i.e. a filled in absorption line due to an active chromosphere.

Further evidence of such activity is seen at secondary eclipse where a strong increase of the Hα absorption line strength is observed. If the spectrum of the secondary star is indeed flat near Hα, the eclipse acts to essentially reduce the observed continuum level of the system, thereby making the lines of the primary deeper. However, the increase in Hα line strength is a factor of 1.6 greater than that expected from a star with the same spectral type as the secondary and with a "flat" spectrum at 6563 Å. This increase is too large to be explained without assuming substantial emission to be present in the secondary star on the eclipsed hemisphere resulting in an Hα line shape exceeding above the continuum level. These different conclusions we draw from the observed Hα equivalent width at secondary eclipse on the one hand and the Hα line shape during primary eclipse on the other hand imply an inhomogeneous distribution of chromospheric plage on the secondary star.

When excluding data taken during eclipses and suspected transient events (phase 0.85) the Hα variations do show a hint of rotational modulation (40% variation) with a maximum EW near phase 0.8 and minimum EW near phase 0.3. We do not know for a certain whether the origin of this variation (if it is indeed real) originates with surface features on the primary or on the secondary star. If the chromospheric plages which may be responsible for this variation are located on the primary, then they may be associated with the large photospheric spot found by Doppler imaging and photometry. If, however, the secondary star produces this variation – our preferred interpretation – then the inhomogeneous chromospheric plage distribution suggested above may also be responsible for it. In this case the dominant chromospherically active region is best visible at phase 0.3 and thus located in the vicinity of one of the coronal X-ray sources (see Fig. 10).

We suspect that the dominant active region on the primary star (the large photospheric spot complex), the probable enhanced chromospheric activity of the secondary star, and an intermediate coronal X-ray source are correlated with each other in a physical sense. This is in agreement with the theory of interacting magnetospheres in RS CVn binaries (Uchida & Sakurai 1983). There, it is proposed that coronal activity takes place between the two stars. A comparison of Fig. 10 in this paper with Fig. 1 in the paper by Uchida & Sakurai (1983) suggests that the coronal sources may be related to arcades of magnetic field lines which connect the two stellar magnetospheres with each other.

Acknowledgements. The ROSAT project has been supported by the Bundesministerium für Forschung und Technologie (BMFT) and the Max-Planck-Gesellschaft (MPG). LP and AH acknowledge the support of the Deutsche Forschungsgemeinschaft (DFG) grant 436 UNG-17/6/93 and Hungarian grant OTKA 829. APH acknowledges the support of NSF grant AST-9315115.

References

Barrado D., Fernández-Figuerola M.J., Montesinos B., De Castro E, 1994, A&A 290, 137
Budding E., 1973, Ap. Space Sci. 22, 87
Budding E., Najim N.N., 1980, Ap. Space Sci. 72, 369
Budding E., Zeilik M., 1987, ApJ 319, 827
Cellino A., Scaltriti F., Busso M., 1985, A&A 144, 315
Dempsey R.C., Linsky J.L., Fleming T.A., Schmitt J.H.M.M., 1993, ApJS 86, 599
Donati J.-F., Brown S.F., Semel M., Rees D.E., Dempsey R.C., Matthews J.M., Henry G.W., Hall D.S., 1992, A&A 265, 682.
Eaton, J.A., 1992, in Surface Inhomogeneities on Late-type Stars, eds. P. B. Byrne and D.J. Mullan, Springer-Verlag, Berlin, Heidelberg, p. 15.
Hempelmann A., Schmitt J.H.M.M., Schultz M., Rüdiger G., Stępień K., 1995, A&A 294, 515
Hempelmann A., Schmitt J.H.M.M., Stępień K., 1996, A&A 305, 284
Hempelmann A., Schöneich W., 1987, Astron. Nachr. 308, 201
Hilditch R.W., Harland D.M., Mc Lean B.J., 1979, MNRAS 187, 797
Kürster M., Dennerl K., 1993, in Physics of Solar and Stellar Coronae, eds. J.F. Linsky & S. Serio, Kluwer, Dordrecht, p. 443
Kurucz R., 1979, ApJS 40, 1.

Lang K.R., 1974, 'Astrophysical Formulae', Springer-Verlag Berlin etc.
McCarthy J., Sandiford B., Boyd D., Booth J., 1993, PASP 105, 881.
Montesinos B., Jordan C., 1988, in A Decade of UV Astronomy with the IUE satellite 1, 238
Noyes R.W., Hartmann L.W., Baliunas S.C., Duncan D.K., Vaughan A.H., 1984, ApJ 279, 763
Ottmann R., Schmitt J.H.M.M., Kürster M., 1993, ApJ 413, 710
Pallavicini R., 1989, A&AR 1, 77
Patkós L., 1982, Comm. Konkoly Obs. No 80, 1
Patkós L., Hempelmann A., 1994, A&A 292, 119
Pfeffermann E., 1986, et al., SPIE, 733, 519.
Stępień K. 1989, A&A 210, 273
Strassmeier K.G., 1990, ApJ 348, 682
Strassmeier K.G., Hall D.S., Fekel F.C., Scheck M., 1993, ApJS 100, 173
Trümper J., et al., 1991, Nature 349, 579
Tsuneta S., Lemen J.R., 1993, in Physics of Solar and Stellar Coronae, eds. J.F. Linsky & S. Serio, Kluwer, Dordrecht, p. 113
Uchida Y., Sakurai T., 1983, in Activity in Red Dwarf Stars, eds. P.B. Byrne & M. Rodono, p. 629
Vogt S.S., 1981, ApJ 250, 327
Vogt S.S., 1988, in The Impact of Very High S/N Spectroscopy on Stellar Physics, eds. G.C. de Strobel & M. Spite, p.253
Vogt S.S., Penrod G.D., Hatzes A.P., 1987, ApJ 321, 496
Vogt S.S., Hatzes A.P., 1991, in The Sun and Cool Stars: Activity, Magnetism, Dynamos, eds. I. Tuominen, D. Moss & G. Rüdiger, p.297
Walter F.M., Gibson D.M., Basri G.S., 1983, ApJ 267, 665
White N., Shafer R., Horne K., Parmar A., Culhane J., 1990, ApJ 350, 776
Zeilik M., De Blasi C., Rhodes M. and Budding E., 1988, ApJ 332, 293
Zimmermann H.U., Becker W., Belloni T., Döbereiner S., Izzo C., Kahabka P., Schwendtker O., 1994, *EXSAS User's Guide*, MPE Report No. 257

This article was processed by the author using Springer-Verlag LaTeX A&A style file *L-AA* version 3.